PCCP

Accepted Manuscript

ROYAL SOCIETY OF CHEMISTRY

www.rsc.org/pccp

The atomic-scale nucleation mechanism of NiTi metallic glasses upon isothermal annealing studied via molecular dynamics simulations

Yang Li , JiaHao Li*, BaiXin Liu

Key Laboratory of Advanced Materials (MOE), School of Materials Science and Engineering, Tsinghua University, Beijing 100084, China

ABSTRACT

Nucleation is one of the most essential transformation paths in phase transition and exerts a significant influence on the crystallization process. Molecular dynamics simulations were performed to investigate the atomic-scale nucleation mechanisms of NiTi metallic glasses upon devitrification at various temperatures (700 K, 750 K, 800 K, and 850 K). Our simulations reveal that at 700 K and 750 K, the nucleation is polynuclear with high nucleation density, while at 800 K it is mononuclear. The underlying nucleation mechanisms have been clarified, manifesting that the nucleation can be induced either by the initial ordered clusters (IOC) or by the other precursors of nuclei evolved directly from the supercooled liquid. The IOC and other precursors stem from the thermal fluctuations of bond orientational order in supercooled liquids during the quenching process and during the annealing process, respectively. The simulation results not only elucidate the underlying nucleation mechanisms varied with temperature, but also unveil the origin of nucleation. These discoveries offer new insights into the devitrification mechanism of metallic glasses.

Keywords: nucleation, molecular dynamics simulation, NiTi metallic glasses

* Corresponding author: lijiahao@mail.tsinghua.edu.cn

1. Introduction

Owing to the excellent mechanical strength, high toughness, and superior soft magnetic properties, nanocrystalline materials have attracted considerable interest from scientists and engineers.[1-3] Besides the solidification of metallic liquids, the devitrification by annealing metallic glasses provides a promising way to fabricate nanostructured alloys.[3] The nanocrystallization of devitrified metallic glasses implies a high nucleation density (up to 10^{23}-10^{24} m^{-3} in bulk metallic glasses) at the initial stage of the crystallization process in deep supercooled conditions.[4] The high density nucleation is difficult to explain in the framework of classical nucleation theory.[2,5] Massive efforts have been devoted to probing the nucleation mechanism experimentally.[4,6-10] For instance, based on the experimental observation of the devitrification of $Zr_{41.2}Ti_{13.8}Cu_{12.5}Ni_{10.0}Be_{22.5}$ (Vit1) and $Zr_{65}Ni_{25}Ti_{10}$ glasses, Liu et al.[4] found that in deep supercooled liquids, nuclei originate from the imperfect ordered packing clusters in initial metallic glasses. Wang et al.[9] reported that the icosahedral ordered clusters in Vit1 act mainly as obstacles to nucleation, leading to the high thermal stability of Vit1. Although the experimental explorations indicated some nucleation mechanisms, the temporal and spatial resolutions of experimental observations are limited, causing that the experiment can't offer detailed images of nucleation at atomic-scale.

Compared with experimental methods, atomistic simulations (Monte Carlo simulations and molecular dynamics simulations) have been frequently used to investigate the nucleation process, owing to their atomic-scale resolution in structure

and dynamics analyses.[11-18] Extensive simulation studies have focused on the nucleation of supercooled liquids,[15-18] suggesting that nucleation originates from either the density fluctuations or bond orientational order fluctuations, i.e. either of the fluctuations promotes the formation of nucleus precursors (preordered regions that trigger the nucleation process).[17,18] However, in deep supercooled liquids, which of the two fluctuations facilitates the precursor remains controversial. The absence of directed simulation studies on the nucleation in deep supercooled metallic liquids and the deficiency of experimental explorations stimulate us to investigate the homogeneous nucleation of metallic glasses upon devitrification through molecular dynamics (MD) simulations.

The devitrification of NiTi metallic glasses is frequently used to fabricate the NiTi shape memory alloys.[19] Due to its importance in technology, NiTi metallic glass is selected as a realistic model to investigate the crystallization of devitrified metallic glasses. First, the crystallization processes at different temperatures were inspected to observe the nucleation of the metallic glasses upon devitrification as well as the structural evolution. Then, the nucleation processes were analyzed in detail to investigate the nucleation mode and mechanism. In the end, the underlying origin of nucleation was elucidated. The simulation results not only unveil the homogeneous nucleation mechanisms of NiTi metallic glasses upon devitrification at various temperatures, but also reveal the origin of nucleation, providing new insights to the nanocrystallization of devitrified metallic glasses.

2. Simulation methods

In this work, we perform MD simulations utilizing Large-scale Atomic/Molecular Massively Parallel Simulator (LAMMPS) packages[20] to investigate the nucleation mechanism of NiTi metallic glasses upon isothermal annealing. The Ni-Ti potential employed in the MD simulations was adopted from the widely used potential developed by Lai[21]. The initial simulation model was set as the B2 ($Pm\bar{3}m$) NiTi structure, consisting of 26 × 26 × 26×2 = 35152 atoms. Periodic boundary conditions were set in *x*, *y*, and *z* axes. The B2 structured model was first melted at 2500 K and annealed isothermally for 8 nanoseconds (timestep: 2 femtoseconds) to equilibrate the molten liquid. The relaxed liquid was then quenched rapidly from 2500 K to 300 K (ambient temperature) at the rate of 2.75×10^{12} K/s and afterwards relaxed for 8 nanoseconds (ns) at 300 K to obtain the $Ni_{50}Ti_{50}$ metallic glass. 20 atomic configurations of metallic glasses were sampled by taking a snapshot of atomic configuration every 20000 timesteps (40 ps) after the metallic glasses relaxed for 8 ns. Each of the sampled atomic configurations was then used to start an independent simulation of annealing. To minimize the induction of nucleation during the heating processes, the temperatures of the metallic glasses were rescaled to the desired temperatures (700 K, 750 K, 800 K, and 850 K) from 300 K with an approximate equivalent heating rate of 2.2×10^{13} K/s. Afterwards, the sampled $Ni_{50}Ti_{50}$ metallic glasses were annealed isothermally for 10 ns to inspect the nucleation process. Although metallic glasses were heated through direct rescaling of temperature, the metallic glasses could be considered as deep supercooled liquids after relaxing for 40 ps (the temperature reached equilibrated). The temperature

and pressure were controlled with Nose-Hoover thermostat and barostat, respectively. All MD simulations ran at zero pressure to exclude the effect of pressure on the nucleation.

3. Structure analysis methods

To identify the crystalline clusters, we used cluster analyses, which are based on the local bond orientational order parameter[22,23]. First, a complex vector $q_{lm}(i)$ is defined for atom i as

$$q_{lm}(i) = \frac{1}{N_b(i)} \sum_{j=1}^{N_b(i)} Y_{lm}(\hat{r}_{ij}) \tag{1}$$

where $Y_{lm}(\hat{r}_{ij})$ are the spherical harmonics of the polar angles defined by the vector $\hat{r}_{ij}$ between atoms i and j. l is a free integer parameter and determines the symmetry to which $q_{lm}(i)$ is sensitive, *e.g.*, $q_{6m}(i)$ is sensitive to local 6-fold symmetry in three-dimensional space. m is an integer that runs from $m = -l$ to $m = l$, and $N_b(i)$ denotes the number of neighbors for an atom i, which are the atoms located within the cutoff distance (3.6 Å in the present simulations, corresponding to the first minimum of pair-correlation functions $g(r)$ of the metallic glasses). Then, we use a normalized component vector $\tilde{q}_{6m}(i)$ ($l = 6$) to define the structural order parameter $S_6(i)$[24,25]

$$\tilde{q}_{6m}(i) = \frac{q_{6m}(i)}{\left[\sum_{m=-6}^{6} |q_{6m}(i)|^2\right]^{1/2}} \tag{2}$$

$$S_6(i) = \sum_{j=1}^{N_b(i)} \sum_{m=-6}^{6} \tilde{q}_{6m}(i) \tilde{q}^{*}_{6m}(j) \tag{3}$$

where $\tilde{q}_{6m}^{*}$ stands for the conjugate vector of $\tilde{q}_{6m}$. The atoms with S_6 larger than 6.5 are defined as crystalline atoms. In the B2 structure, each atom is surrounded by 14 coordination atoms (8 in the first neighbor shell and 6 in the second neighbor shell) in the cutoff distance of 3.6 Å. It is considered that the atoms *i* and *j* are "connected", if $\sum_{m=-6}^{6} \tilde{q}_{6m}(i)\tilde{q}_{6m}^{*}(j) > 0.5$.[24] When the "connected" atoms are more than 13, the central atom can be considered as crystalline atoms, indicating that the threshold of S_6 is determined as 6.5. The choice of S_6 threshold not only ensures the excellent distinction between crystalline atoms and liquid-like atoms (or glassy atoms) but also includes the atoms at the liquid-solid interface as crystalline atoms. The probability distributions of structural order parameter S_6 for amorphous metallic glasses, partially crystallized glasses (crystallinity χ = 0.5, 0.8) and B2 crystals are given in Figure S1 in Supplementary Information, exhibiting the accurate distinguishing between metallic glasses and crystals. By increasing the threshold of S_6, the number of crystalline atoms will decrease, but the cluster analyses based on S_6 indicate similar nucleation trends. The details on S_6 can refer to Ref. 17, 24 and 25. When the distance between two crystalline atoms is less than the cutoff radius (3.6 Å), they are considered to be in the same crystalline cluster. The aggregated crystalline atoms form the crystalline clusters that are consider to be embryos (smaller than a critical nucleus) or nuclei (equivalent to or larger than a critical nucleus).

Furthermore, to measure the bond orientational order of the precursor region, we employ the spatially averaged bond orientational parameter $Q_6(i)$[23], which is defined as

$$Q_6(i) = \sqrt{\frac{4\pi}{13}\sum_{m=-6}^{6}\left|\hat{q}_{6m}(i)\right|^2} \quad (4)$$

where $\hat{q}_{6m}(i)$ is denoted as

$$\hat{q}_{6m}(i) = \frac{1}{N_b(i)}\sum_{k=0}^{N_b(i)} q_{6m}(k) \quad (5)$$

In addition, the pair-correlation functions $g(r)$[26], angle distribution functions P(θ)[26] and Voronoi tessellations[27] are employed to give a clear and explicit description of the structures of metallic glasses and nuclei. In Voronoi tessellations, the Voronoi polyhedron is composed of the planes that perpendicularly bisect each line connecting the central atom and its neighbor atoms. The Voronoi index, $<n_3, n_4, n_5, n_6>$, where n_i denotes the number of *i*-edged faces of the Voronoi polyhedra, is used to designate the type of the Voronoi polyhedron and the characteristics of the atomic cluster enclosing the centered atom. The details on the analyses can refer to Ref. 26. Based on the Voronoi polyhedron volume derived from Voronoi tessellations, the local atomic density ρ_i of atom *i* can be calculated as $\rho_i = 1/v_i$, where v_i represents the Voronoi polyhedron volume of atom *i*.[17]

4. Results and discussion

4.1 Overview of the nucleation and structural evolution

Nucleation is the initial stage of crystallization and greatly influences the crystallization process. First, the energies of the NiTi metallic glasses upon isothermal annealing at different temperatures were monitored to check whether the crystallization occurred. Figure 1 exhibits the evolution of potential energy as well as the number of

crystalline atoms during the annealing process. It should be noted that the repeated simulations based on different atomic configurations of metallic glasses reveal similar crystallization process, so typical energy evolution and the corresponding variation of number of crystalline atoms are presented in Figure 1. The energy variation indicates that the metallic glasses crystallized with the decrease of potential energy when devitrified at 700 K, 750 K, and 800 K, while at 850 K, no crystallization was observed during the annealing process as the potential energy and the number of crystalline atoms almost remained unchanged. The crystallization at temperatures below 850 K during annealing was confirmed with the increase of number of crystalline atoms as shown in Figure 1. The three growth curves of number of crystalline atoms signify that the crystallization rate of metallic glasses upon devitrification increases with the annealing temperature (700 K to 800 K), which is confirmed by the fact that the decreasing rate of potential energy increases with temperature. The absence of crystallization at 850 K reveals that the homogeneous nucleation is so difficult to occur at 850 K in the supercooled liquid that the induction time is beyond the observation time (10 ns). In the following part we'll focus on the nucleation processes at different temperatures (700 K, 750K, and 800 K).

Besides the energy variation, the structural analyses based on the pair correlation functions, angle distribution functions and Voronoi tessellations were conducted to acquire the detailed structural information of the devitrified metallic glasses during the nucleation process. Figures 2 and 3 present the structural features of the initial glasses and the nuclei, respectively. Figure 2(a) shows the total pair-correlation functions $g(r)$,

the partial pair functions of Ni atoms $g_{Ni\text{-}Ni}(r)$, those of Ni atoms and Ti atoms $g_{Ni\text{-}Ti}(r)$, and those of Ti atoms $g_{Ti\text{-}Ti}(r)$, indicating short range order and long range disorder, which is confirmed by the amorphous feature of angle distribution exhibited in Figure 2(b). Figures 2(c) and 2(d) display the Voronoi indexes of the ten most frequent Voronoi polyhedra around Ni atoms and Ti atoms, respectively. The fractions of ten most frequent Voronoi polyhedra in all the Voronoi polyhedra are all less than 1.5 %, indicating structural complexity and variety of NiTi metallic glasses. The insets in Figures 2(c) and 2(d) denote the 3D atomic configurations of the most frequent Voronoi polyhedra around Ni atoms (<0,2,6,4>) and Ti atoms (<0,2,8,4>), respectively. Although few icosahedra (<0,0,12,0>) are found in the frequent Voronoi polyhedra, the characteristic polyhedra (<0,2,6,4>, <0,2,8,2>, <0,2,8,4> and so on) indicate the local fivefold symmetry of the metallic glasses. Figure 3(a) exhibits the $g(r)$, $g_{Ni\text{-}Ti}(r)$, and $g_{Ti\text{-}Ti}(r)$ of nuclei, as well as the $g(r)$ of ideal B2 crystal with the same lattice parameters (3.05 Å). The good conformity between the $g(r)$ of nuclei and B2 crystal as well as the good consistency between $g_{Ni\text{-}Ti}(r)$ and $g_{Ti\text{-}Ti}(r)$ reveals that the nuclei possess a typical B2 ($Pm\bar{3}m$) structure, which is further validated by the accordance between the angle distribution of the nuclei and that of B2 crystal as shown in Figure 3(b). Figures 3(a) and 3(b) manifest that the nuclei have transformed from the initial disordered glasses to the ordered B2 NiTi crystals, agreeing with the experimental observations of NiTi metallic glasses upon devitrification[28]. To analyze the structural evolution of short-range order, the Voronoi tessellation analyses of nuclei are revealed in Figure 3(c) and Figure 3(d), indicating that the dominating Voronoi polyhedra around Ni atoms and Ti

atoms are both <0,6,0,8> and the corresponding factions are more than 50%. The atomic configurations of <0,6,0,8> polyhedra exhibited in the insets in Figures 3(c) and 3(d) indicate the ordered body-centered cubic structure (B2), conforming to the structure analyses exhibited in Figures 3(a) and 3(b). The dominating <0,6,0,8> polyhedra also manifest the local fourfold and sixfold symmetries of nuclei that are distinguished from the local fivefold symmetry of metallic glasses.

4.2 Nucleation density and mode

To investigate the detailed nucleation processes during the devitrification at different temperatures, one first needs to find a way to determine the critical nucleus. It is reported that the mean first-passage-time (MFPT) method can effectively derive the induction time and number of atoms or size n_c of the critical nucleus from MD simulations of nucleation.[12,29] In the present study, the n_c of nucleation occurred at 700 K, 750 K, and 800 K are computed to be 62, 33, and 23. The derived sizes of critical nuclei are comparable with those derived from other MD simulations[2,5] and the fitting data were in excellent consistency with the MFPT equations, revealing that our calculation of critical nucleus sizes is reasonable and valid.

Based on the critical nucleus size, the (post-critical) nuclei and embryos can be distinguished and the nucleation density can be analyzed. The evolution of nucleus numbers during the homogeneous nucleation at 700 K, 750 K and 800 K with the corresponding snapshots of nuclei at 0.5 ns is reported in Figure 4. The variation of nucleus numbers at 700 K and 750 K implies a tendency of first increase and then decrease with trivial fluctuations, indicating the nucleus numbers have maximum value.

The increase of nucleus numbers signifies the proceeding of nucleation while the decrease suggests the impingement of nuclei, leading to the final large combined nucleus. The fluctuations stem from the stochastic feature of nucleation, that is, a nucleus can either grow or dissolve. The maximum numbers of nuclei at 700 K, 750 K and 800 K are 16, 6 and 1, respectively, suggesting the nucleation density decreases as temperature increases. The nucleation density at 750 K are estimated to be 1.16×10^{25} m^{-3}, which is close to the high nucleation density (10^{24} m^{-3}) in bulk metallic glasses observed in experiment[4]. The experimental nucleation density of devitrified NiTi amorphous thin films varied from 10^{18} to 10^{19} m^{-3} at around 750 K.[30-33] The high nucleation density observed in MD simulations is several orders of magnitude higher than experimental observations in thin films. The inconsistency originates from the low spatial resolution of micrometers in the experimental observations compared with simulations and the ignoring of nuclei in the direction perpendicular to the film plane in experiment, leading to the underestimation of the nucleation density (several orders of magnitude). The limitation of the simulation size and the microscopic uniformity of Ni atoms and Ti atoms contribute to the overestimation of nucleation density in simulation. In fact, the simulation results of nucleation are frequently higher than the experimental observations and our calculated nucleation density is comparable with that in the molted sodium chloride[34], indicating our simulation results are reasonable. Figure 4(b), 4(c) and 4(d) show the snapshots of nuclei at 0.5 ns at 700 K, 750 K, and 800 K, respectively. The nuclei are crystalline clusters that are larger than the corresponding critical nucleus size n_c. Figure 4(d) indicates the (111) crystallographic

plane of a B2 NiTi nanocrystal. It is found that the number of nuclei at 700 K is the most, that at 750 K is less, and that at 800 K is the least (only one). The numbers of nuclei at different temperatures signify that the nucleation has transformed from the polynuclear mode (700 K and 750 K) to mononuclear mode (800 K). To understand the origin of the two nucleation modes, one needs to inspect the atomistic mechanism of nucleation.

4.3 Atomistic mechanism of nucleation

To obtain an in-depth understanding on the atomistic mechanism of nucleation, the evolution of nuclei needs to be analyzed in detail. We first traced the trajectories of the nuclei. The nuclei are always evolved from embryos. It is found that though they have a small proportion in the whole metallic glass, the initial ordered atomic clusters (IOC) have a significant impact on the nucleus evolution. Figure 5 exhibits the snapshots of the embryos or nuclei in initial metallic glass and those in metallic glass devitrified at 700 K for 100 ps, 300 ps and 500 ps. Figure 5(a) indicate there exist a few IOC in the initial metallic glass. It should be noted that although IOC are related to the quenching rate during the preparation of metallic glasses, the MD simulations at various quenching rates (even up to 10^{12} K/s) reveal that IOC always exist in metallic glasses after enough equilibration. The embryo and nucleus evolution at 700 K are presented in Figures 5(b), 5(c) and 5(d), in which the red atoms denote the ordered atoms inherited from IOC. One can find that the inherited ordered atoms act as the pre-nuclei, indicating that IOC can be considered as the preexistent embryos or precursors of nuclei for the subsequent nucleation and crystal growth. It should be noticed that the IOC frequently

comprise several atoms (less than 20 atoms) with the size of several unit cells of crystal, exhibiting a characteristic short-range order. The inheritance of characteristic order from IOC reduces the free energy barrier for nucleation and promotes the nucleation, contributing to the polynuclear nucleation and high nucleation density at 700 K. Upon further inspection on Figures 5(b), 5(c) and 5(d), it is found that not all the IOC evolve into stable nuclei due to the destruction of thermal fluctuations, revealing that part of the precursors are IOC and the other precursors evolve directly from the liquid.

The nucleation scenario at 750 K revealed in Figures 6(a) and 6(b) is similar to that at 700 K, in which two of the nuclei evolve from IOC while the others evolve directly from the liquid phase. With the contribution of IOC to the nucleation, both the nucleation scenarios are polynuclear. The nuclei evolution at 800 K shown in Figures 6(c) and 6(d) implies the absence of ordered atoms inherited from IOC, leading to the high free energy barrier for nucleation and the mononuclear nucleation. The dissolution of IOC at higher temperatures indicates that IOC are inherently thermodynamically unstable. The destruction of IOC is caused by the thermal fluctuations at 800 K that are correlated with the atomic diffusivity. The self-diffusivity coefficients of Ni and Ti in the supercooled NiTi liquids at various temperatures are displayed in Figure S2 in Supplementary Information. As the temperature increases, the self-diffusivity coefficients grow exponentially. At 800 K, the high atomic diffusivity leads to the breaking down of IOC and the transformation of nucleation modes.

The nucleation scenarios at 700 K, 750 K and 800 K unveil two nucleation mechanisms: the first is the nucleation induced by IOC, contributing to the polynuclear

nucleation mode and high nucleation density at relatively low temperatures (700 K and 750 K); the second is the nucleation induced by the other precursors evolved directly from the liquid phase, occurring at all temperatures. The first nucleation mechanism is similar to that induced by imperfect ordered packing clusters in bulk metallic glasses[4], suggesting that the IOC-mediated nucleation mechanism is fundamental and universal in metallic glasses. It should be noted that the typical imperfect ordered packing clusters[4] comprise several hundreds of atoms with the size of 1-2 nm that are an order of magnitude larger than IOC. The IOC-mediated nucleation mechanism makes a great contribution to the high nucleation density during nanocrystallization of metallic glasses. Upon further inspection on the preparation of metallic glasses, it is found that the IOC have evolved from the molten liquid during the quenching process, which resembles that the other precursors have evolved directly from the supercooled liquid during the annealing process. As a result, it is considered that all the precursors of nuclei including IOC evolve from the supercooled liquid essentially.

4.4 Origin of nucleation

To acquire an understanding on the origin of the nucleation of metallic glasses upon devitrification, further investigation on the evolution of precursors of nuclei is required. In this section, we take the precursor evolution during the annealing process as an example to elucidate how the precursors evolve from the supercooled liquid and therefore reveal the nucleation origin. As discussed in Section 1, the precursors in the supercooled liquid are considered to be induced either by density fluctuations or bond orientational order fluctuations. To determine the origin of nucleation in supercooled

liquid, the distributions of atomic density and bond orientational order are analyzed. Figures 7(a) and 7(b) show the probability distributions of bond orientational order (Q_6) and atomic density (ρ) of liquid-like atoms (orange solid line) and crystalline atoms (light blue dash dot line) in the metastable liquid (before the critical nuclei emerged) at 800 K. The Q_6 reflects the local sixfold symmetry of the central atom with its neighbors, indicating that the liquid-like atoms with local fivefold symmetry would have low Q_6 while the crystalline atoms with sixfold symmetry would have high Q_6. Figure 7(a) indicates that the Q_6 distributions of crystalline atoms and liquid-like atoms are barely overlapped, signifying the obvious distinction between the bond orientational order of liquid-like atoms and crystalline atoms. Nevertheless, the density distributions of crystalline atoms and liquid-like atoms in Figure 7(b) are overlapped, implying the little difference between the liquid-like atoms and crystalline atoms. The contrast between the distributions of bond orientational order and density reveals that the precursor in the metastable liquid (before the emergence of critical nuclei) originates from the areas of high bond orientational order rather than those of high density, i.e., the nucleation in the metastable liquid is induced by the fluctuations of bond orientational order. To further unveil the coupling between density and bond orientational order, the distributions of structure order S_6 of the atoms in the deep supercooled liquid (before critical nuclei formed) with the Q_6 and ρ coordinates are exhibited in Figure 8. The structural order S_6 increases in an almost continuous way as Q_6 increases, while the dots with similar S_6 have a wide range of density. The contour lines of S_6 with different colors are nearly parallel to the density axis, indicating that the density has little effect on the

structure order and the coupling between density and bond orientational order in the precursors is weak. The variation of structural order parameter with bond orientational order and density unveils that the precursor stems from the high bond orientational region and the nucleation in NiTi supercooled liquid is induced by the fluctuations of bond orientational order, which conforms to the simulation results in supercooled liquid Fe[18]. The conformity confirms the validity of our simulation results. Considering that all the precursors of nuclei evolve from the supercooled liquid, the precursors originate from the bond orientational order fluctuations, revealing that the nucleation of NiTi metallic glasses upon devitrification is induced by the thermal fluctuations of bond orientational order in essence.

5. Conclusions

MD simulations were conducted utilizing LAMMPS to investigate the nucleation mechanism of the NiTi metallic glasses upon devitrification at 700 K, 750 K, 800 K and 850 K. The simulation results indicate the polynuclear nucleation at 700 K and 750 K, the mononuclear nucleation at 800 K, and no nucleation during the observation time at 850 K. The polynuclear nucleation is induced by the initial ordered clusters (IOC) and the other precursors evolved directly from the liquid, while the mononuclear nucleation is induced only by the precursor evolved from the liquid. The IOC-mediated nucleation mechanism is consistent with the experimental observation in bulk metallic glasses, contributing to the high nucleation density of metallic glasses upon devitrification at 700 K and 750 K. Upon further investigation on the formation of IOC,

IOC stem from the fluctuations of bond orientational order (BOO) during the quenching process, while the other precursors of nuclei stem from those BOO fluctuations during the annealing process. The nucleation originated from BOO fluctuations is verified by that in the supercooled Fe, confirming the validity of our simulation results. The simulations not only unveil the underlying nucleation mechanism of devitrified metallic glasses but also elucidate the nucleation origin. Our simulation results can shed new light on the devitrification of metallic glasses.

Acknowledgements

The authors appreciate the financial support from the National Natural Science Foundation of China (51131003), the Ministry of Science and Technology of China (973 Program 2011CB606301, 2012CB825700) and the Administration of Tsinghua University.

References:

1 A. L. Greer, *Nature*, 1994, **368**, 688-689.

2 K. Lu, *Mater. Sci. Eng. R.*, 1996, **16**, 161-221.

3 M. T. Clavaguera-Mora, N. Clavaguera, D. Crespo, and T. Pradell, *Prog. Mater. Sci.*, 2002, **47**, 559-619.

4 X. J. Liu, G. L. Chen, H. Y. Hou, X. Hui, K. F. Yao, Z. P. Lu, and C. T. Liu, *Acta Mater.*, 2008, **56**, 2760-2769.

5 H. Assadi and J. Schroers, *Acta Mater.*, 2002, **50**, 89-100.

6 J. Schroers, Y. Wu, R. Busch, and W. L. Johnson, *Acta Mater.*, 2001, **49**, 2773-2781.

7 X. L. Wang, J. Almer, C. T. Liu, Y. D. Wang, J. K. Zhao, A. D. Stoica, D. R. Haeffner, and W. H. Wang, *Phys. Rev. Lett.*, 2003, **91**, 265501.

8 T. A. Waniuk, R. Busch, W. L. Johnson, and A. Masuhr, *Phys. Rev. Lett.*, 1999, **82**, 2290.

9 Q. Wang, C. T. Liu, Y. Yang, Y. D. Dong, and J. Lu, *Phys. Rev. Lett.*, 2011, **106**, 215505.

10 Y. T. Shen, T. H. Kim, A. K. Gangopadhyay, and K. F. Kelton, *Phys. Rev. Lett.*, 2009, **102**, 578015.

11 J. Anwar and D. Zahn, *Angew. Chem. Int. Ed.*, 2011, **50**, 1996-2013.

12 P. Yi and G. C. Rutledge, *Annu. Rev. Chem. Biomol.*, 2012, **3**, 157-182.

13 X. Tang, Z. Xie, T. Yin, J. Wang, P. Yang, and Q. Huang, *Phys. Chem. Chem. Phys.*, 2013, **15**, 16314-16320.

14 V. Daskalakis, F. Charalambous, F. Panagiotou, and I. Nearchou, *Phys. Chem. Chem.*

Phys., 2014, **16**, 23723-23734.

15 D. Moroni, P. R. Ten Wolde and P. G. Bolhuis, *Phys. Rev. Lett.*, 2005, **94**, 235703.

16 T. Schilling, H. J. Schoepe, M. Oettel, G. Opletal, and I. Snook, *Phys. Rev. Lett.*, 2010, **105**, 257012.

17 J. Russo and H. Tanaka, *Sci. Rep.-Uk*, 2012, **2**, 505.

18 R. Li, Y. Wu and J. Xiao, *J. Chem. Phys.*, 2014, **140**, 34503.

19 Y. Fu, H. Du, W. Huang, S. Zhang, and M. Hu, *Sensors and Actuators A*, 2004, **112**, 395-408.

20 S. Plimpton, *J. Comput. Phys.*, 1995, **117**, 1-19.

21 W. S. Lai and B. X. Liu, *J. Phys.: Condens. Matter*, 2000, **12**, L53.

22 D. R. Nelson, M. Ronchetti and P. J. Steinhardt, *Phys. Rev. B*, 1983, **28**, 784-805.

23 W. Lechner and C. Dellago, *The Journal of Chemical Physics*, 2008, **129**, 114707.

24 P. Rein Ten Wolde, M. J. Ruiz-Montero and D. Frenkel, *J. Chem. Phys.*, 1996, **104**, 9932.

25 G. C. Sosso, G. Miceli, S. Caravati, F. Giberti, J. Behler, and M. Bernasconi, *J. Phys. Chem. Lett.*, 2013, **4**, 4241-4246.

26 Y. Q. Cheng and E. Ma, *Prog. Mater. Sci.*, 2011, **56**, 379-473.

27 H. W. Sheng, W. K. Luo, F. M. Alamgir, J. M. Bai, and E. Ma, *Nature*, 2006, **439**, 419-425.

28 K. T. Liu and J. G. Duh, *J. Non-Cryst. Solids*, 2007, **353**, 1060-1064.

29 S. E. M. Lundrigan and I. Saika-Voivod, *J. Chem. Phys.*, 2009, **131**, 104503.

30 H. Lee, H. Ni, D. T. Wu, and A. G. Ramirez, *Appl. Phys. Lett.*, 2005, **87**, 114102.

31 H. Ni, H. Lee and A. G. Ramirez, *J. Mater. Res.*, 2005, **20**, 1728-1734.

32 H. Lee, H. Ni, D. T. Wu, and A. G. Ramirez, *Appl. Phys. Lett.*, 2005, **87**, 124102.

33 T. LaGrange, D. S. Grummon, B. W. Reed, N. D. Browning, W. E. King, and G. H. Campbell, *Appl. Phys. Lett.*, 2009, **94**, 184101.

34 C. Valeriani, E. Sanz and D. Frenkel, *J. Chem. Phys.*, 2005, **122**, 194501.

Figures

Figure 1. The evolution of potential energy (solid lines) and number of crystalline atoms (dash dot lines) at different temperatures with the increasing of time.

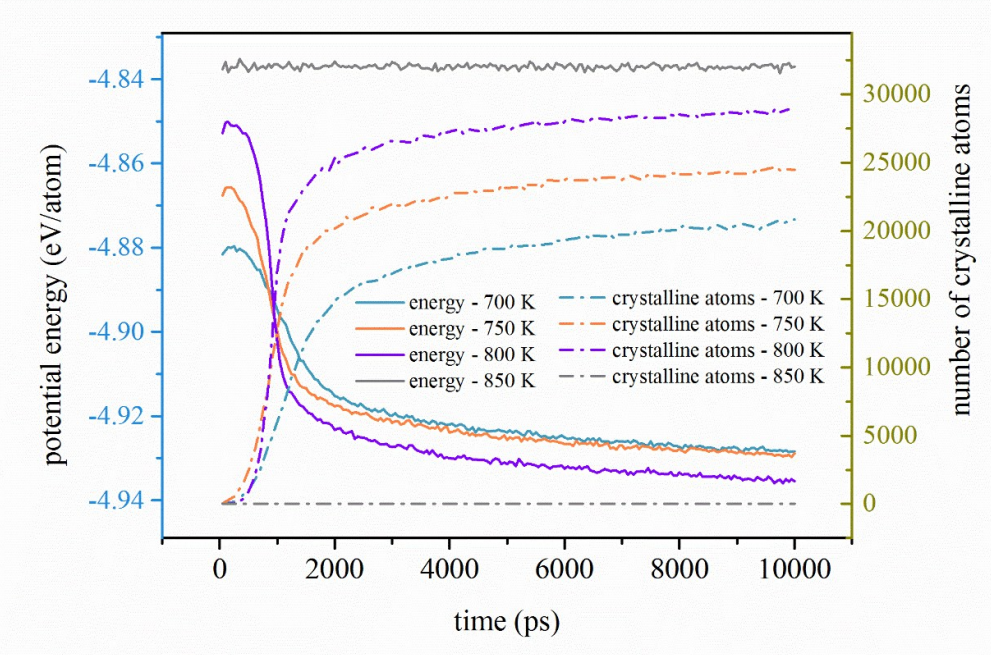

Figure 2. (a) The pair correlation functions and (b) angle distribution function of the initial metallic glass; the fractions of the ten most frequent Voronoi polyhedra around (c) Ni atoms and (d) Ti atoms in the initial metallic glass.

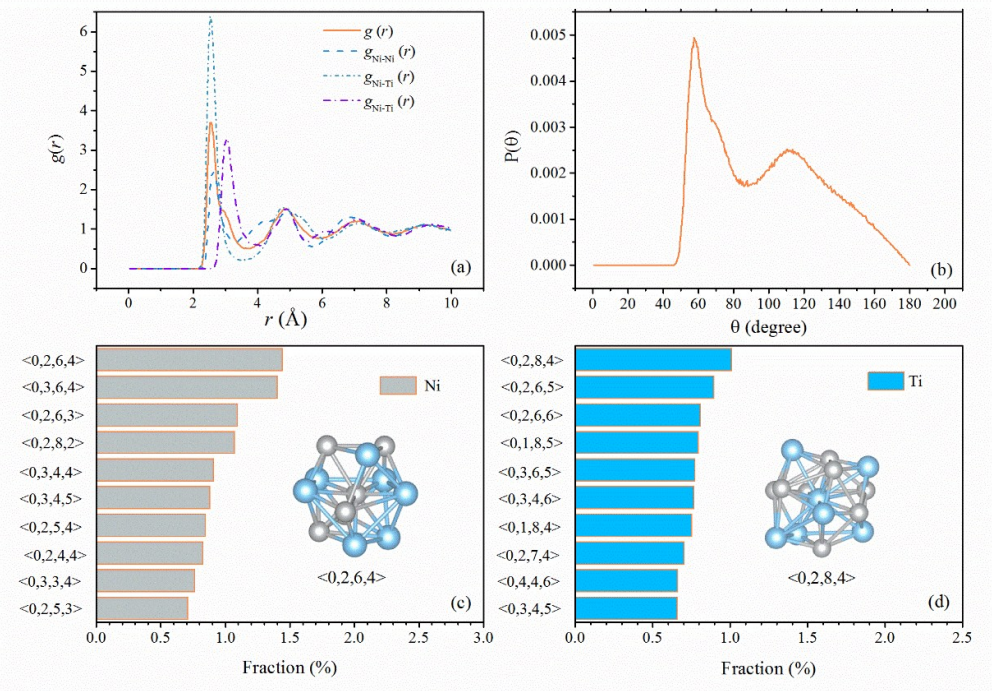

Figure 3. (a) The pair correlation functions and (b) angle distribution functions of the nuclei and the ideal B2 crystal; the fractions of the ten most frequent Voronoi polyhedra around (c) Ni atoms and (d) Ti atoms in the nuclei. The nuclei are selected from the metallic glasses devitrified at 700 K for 2.4 ns. The nuclei in the metallic glasses devitrified at other temperatures reveal similar structural features.

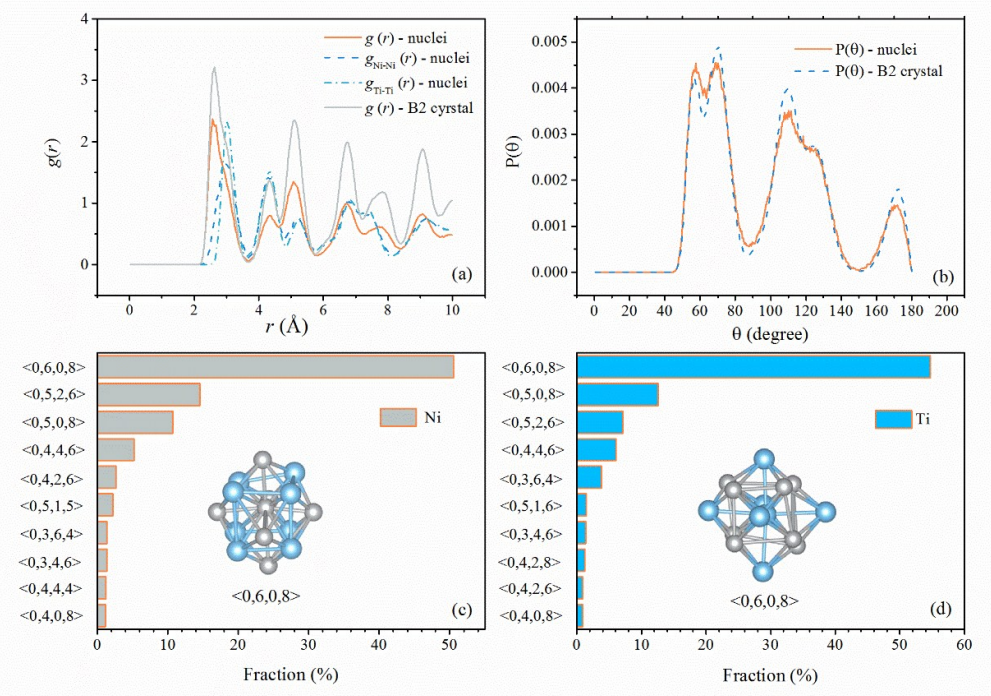

Figure 4. The evolution of (a) nucleus number at different temperatures with time and the corresponding snapshots of nuclei at 0.5 ns at (b) 700 K, (c) 750 K, and (d) 800 K. The coordinates of atoms were shifted according to periodic boundary conditions for visualization.

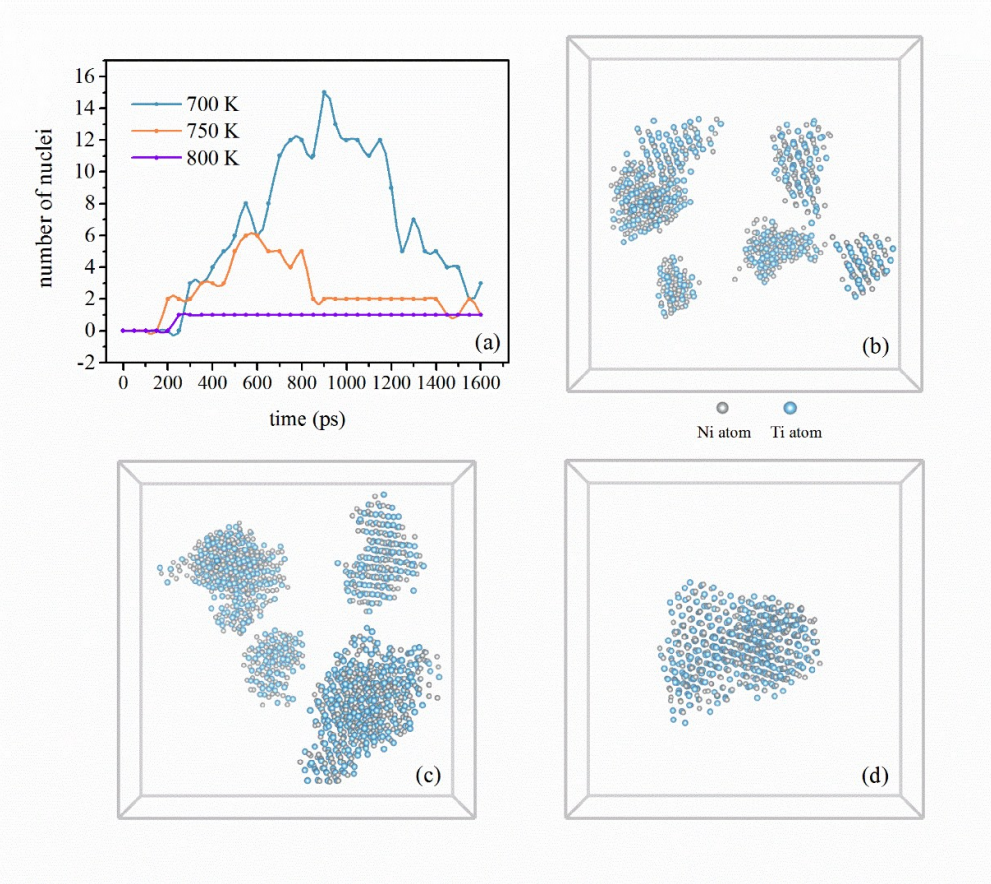

Figure 5. The snapshots of the embryos or nuclei in (a) initial metallic glass (before heating) and in metallic glass annealed at 700 K for (b) 100 ps, (c) 300 ps, and (d) 500 ps. The grey atom indicates a Ni atom, the light blue atom represents a Ti atom, and the red atom denotes an ordered atom that inherited from IOC.

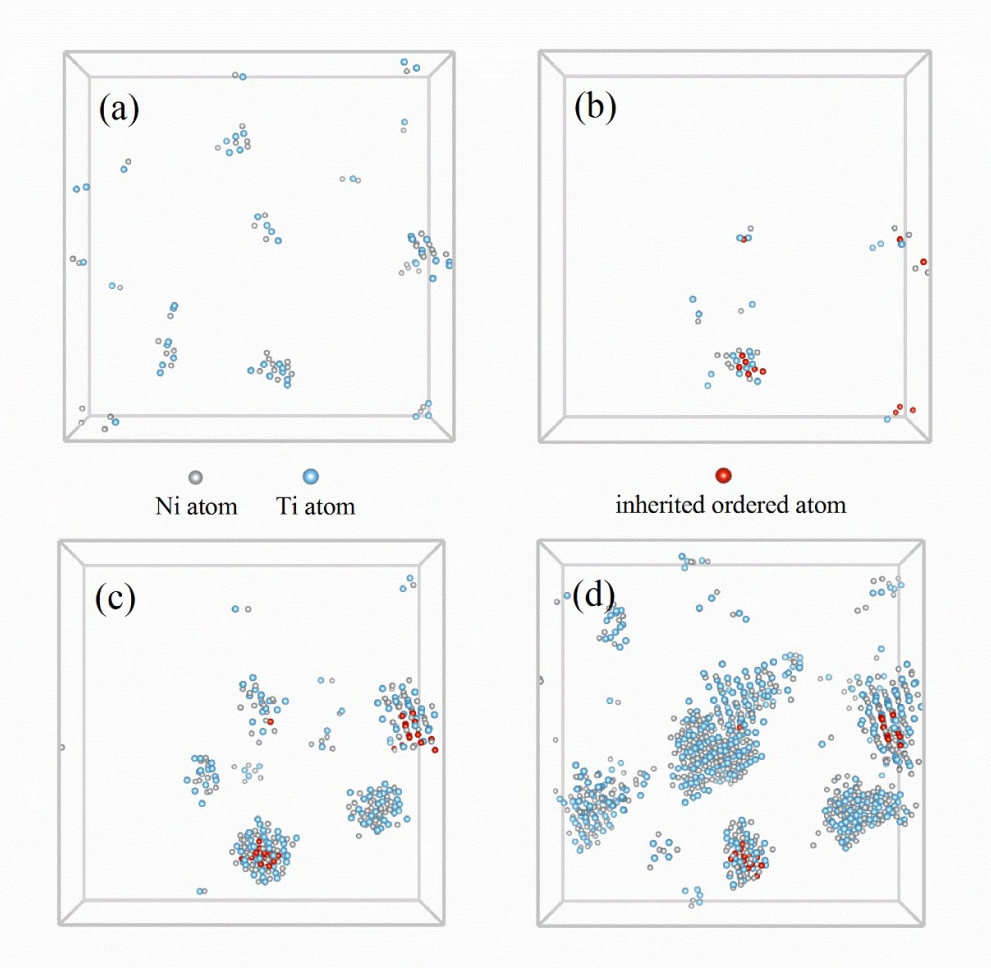

Figure 6. The snapshots of the embryos or nuclei of metallic glasses annealed at 750 K for (a) 200 ps, (b) 500 ps, and those annealed at 800 K for (c) 200 ps, (d) 500 ps.

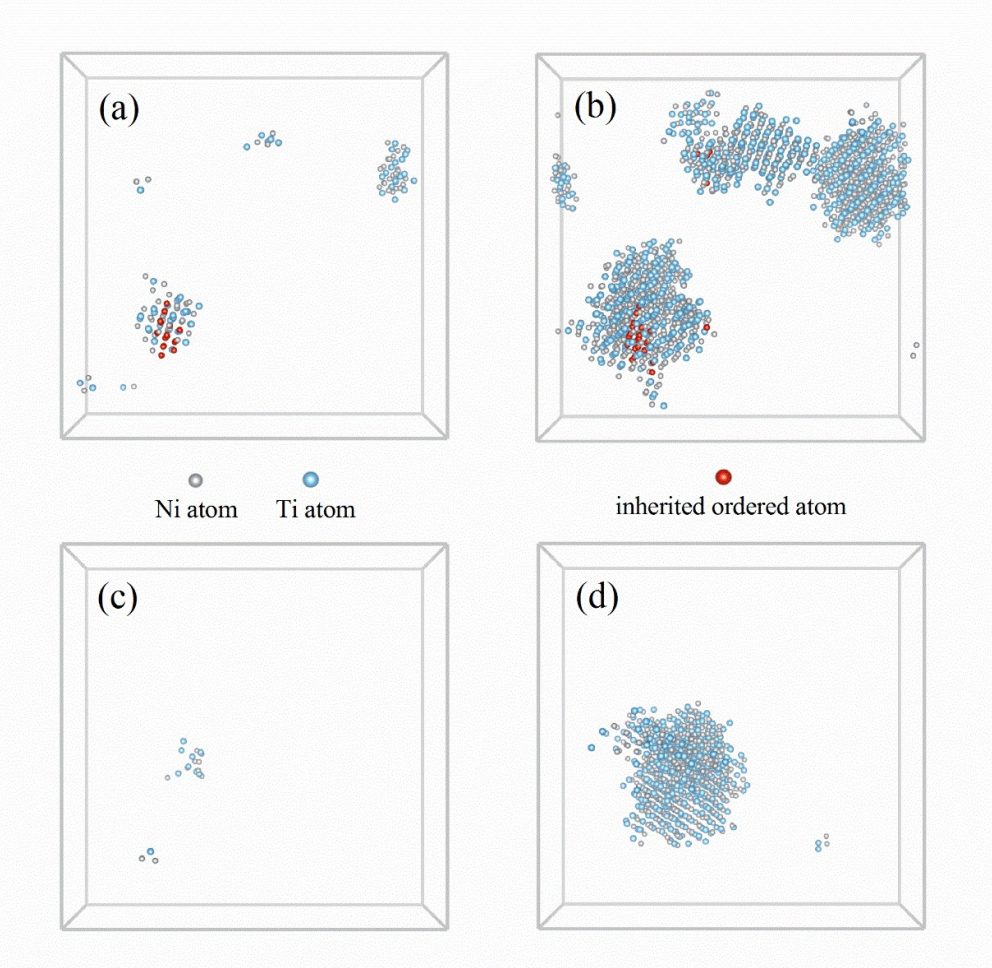

Figure 7. The probability distributions of (a) Q_6 and (b) atomic density ρ (Å^{-3}) of liquid-like atoms (orange solid line) and crystalline atoms (light blue dash dot lines) in the supercooled liquid (before the critical nuclei emerged).

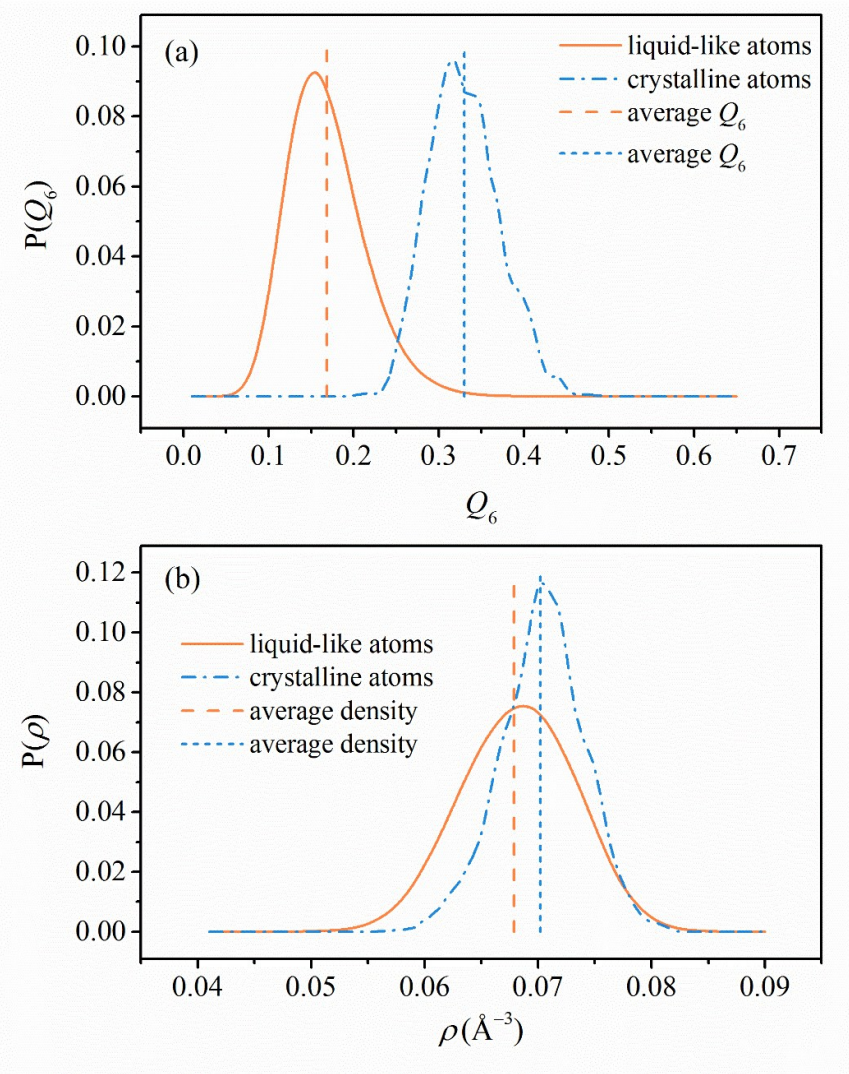

Figure 8. The distributions of S_6 of the atoms in the supercooled liquid (before the critical nuclei appeared) varied with the coordinates of Q_6 and ρ (Å^{-3}).